Organic Semiconductors: Incorporating Xylindein into (Opto)Electronic Devices

Jeremy J. Rath
Advised by: Oksana Ostroverkhova Department of Physics

Oregon State University

2016

Abstract

This research investigates the electronic properties of a fungi-derived pigment, xylindein as a novel sustainable material for organic electronics. Xylindein molecules were characterized in solution and in film. Absorption spectra and (photo)luminescence spectra were taken at various excitation wavelengths. Xylindein's molecular properties were computed with the Gaussian 09 software suite. Pentacene and peri-xanthenoxanthene were used as references for the reliability of the computations. Thin film devices were made to measure the (photo)conductivity at various excitation wavelengths and current-voltage data. Experimental results for anthradithiophene were used for comparison. A lower limit for the charge carrier mobility was estimated to be 0.5 $\frac{\mathrm{cm}^2}{\mathrm{V\,s}}$. Xylindein shows promise for use in both single-component and donor/acceptor solar cells.

Contents

List of Figures

1 Introduction

This section will discuss the current benchmark for and status of organic semiconductors. This section will also discuss several physical phenomena relating to xylindein.

1.1 Motivation

Organic semiconductors are of interest due to their applications in low cost, light weight and flexible electronic devices. They also allow for the fine tuning of optical, and electronic properties when combined with a composite system. Organics in composites have already shown their effectiveness. Composites containing donor and acceptor molecules have been incorporated in organic solar cells [1, 2], light-emitting diodes [3], lasers [4], and photo-refractive devices [5, 6] such as 3D holographic displays [7, 8]. Current organic solar cells utilize hetero-junctions with fullerene acceptors [1, 9] but these are expensive. They also suffer from performance problems such as low optical absorption, photo-chemical and oxygen exposure related degradation, and unwanted chemical reactivity with other components in the solar cell [10, 11, 12]. Thus, non-fullerene donor/acceptor organic solar cells are in great demand. However, they currently can provide power conversion efficiencies only roughly three-quarters (8.5% vs 12%) of those which are provided by fullerenes [13, 14, 15]. Xylindein shows promise to fill this role in donor/acceptor, organic solar cells.

Single-component solar cells use only a donor instead of solar cells utilizing donor-acceptor hetero-junctions. This approach was abandoned in the 1980s due to low power conversion efficiencies. However, it does have the advantage of consistent device performance when compared to donor-acceptor solar cells. This has brought attention back towards the approach [16]. New methods are being developed that would involve polymers that have a high dielectric constant [17, 18] and hydrogen bonded pigments [19]. Xylindein shows promise to fill this role as well as it has both intra- and inter- molecular hydrogen bonds. Xylindein could potentially create ordered films with improved optoelectronic properties due to the presence of its strong bonds.

1.1.1 Kasha's Rule

Kasha's rule states that luminescence will be able to be measured only when an electron moves from the lowest excited state of a given multiplicity [20]. A multiplicity is a collection of states with the same energy. This is derived from the Pauli Exclusion Principle. Exceptions to this rule are not forbidden but, rather, are unlikely. The rule is a consequence of the non-radiative $S_2 \rightarrow S_1$ transition being much faster than the radiative $S_2 \rightarrow S_1$ and $S_2 \rightarrow S_0$ transitions [21]. Figure 1.1 illustrates the standard decay progression of an electron in a molecule that obeys Kasha's rule and an example of a decay progression that violates Kasha's rule. Having all the fluorescence coming from one transition results in the fluorescence spectrum having its peaks at the same wavelength regardless of excitation wavelength—assuming that the excitation energy is higher than the peak location energy. Furthermore, it implies that the absorption is a mirror of the fluorescence because nearly the same transitions will occur just in the opposite direction. There is often a shift between the two highest peaks which is called the Stokes' shift. This shift arises from the vibrational harmonics of the energy states.

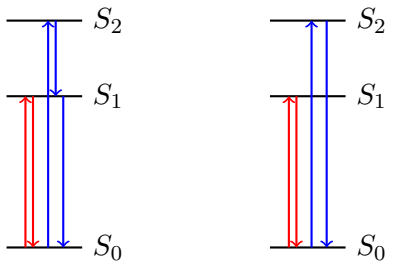

Figure 1.1: Depiction of Kasha's Rule [Left: Obeys | Right: Disobeys]

1.1.2 Pi-Stacking

Systems with π-conjugation have been extensively used in advanced applications such as sensors and in electronics because the π-conjugated materials used can make properties of a system more easily fine tuned [22]. Materials that are π-conjugated have a strong $\pi-\pi$ overlap—an attraction between between molecules. Charge transport relies on the $\pi-\pi$ overlap and, therefore, these materials have a higher charge carrier mobility.

1.1.3 Hydrogen Bonding

Hydrogen bonds are directional, non-covalent interactions between hydrogen and a highly electronegative atom. These atoms include nitrogen, oxygen, or fluorine. Hydrogen bonds are stronger than the more common Van der Waals force. These bonds allow for lone electron pairs to move from a donor to an acceptor which could increase the charge carrier mobility. Because of their precise nature, hydrogen bonds are very useful in the creation of supra-molecular architectures. However, these bonds need to have large association constants to be able to produce a significantly large assembly. H-bonds have already been used to allow for stronger π-conjugated molecules and to adjust their positioning [22].

2 Materials

This section describes the materials used in this project. Matters of most importance are computational complexity, shape, and solid state properties.

2.1 Pentacene

Pentacene, Figure 2.1, is a molecule that is linear in its structure and has been studied extensively. Experiments have shown high values for charge carrier mobility, photoconductivity and luminescence for functionalized variations of pentacene [23]. Pentacene, however, has several drawbacks. Pentacene is not solution processable and has low stability when in contact with oxygen. Pentacene was chosen due to its computational simplicity and the abundance of experimental data.

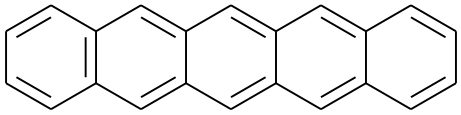

Figure 2.1: Structure of the pentacene molecule

This molecule is computationally simple. It has a structure that extends in one dimension and it contains only carbon and hydrogen. Carbon is only slightly more electronegative than hydrogen and therefore the electrons will stay close to the middle of the bond rather than clinging to one of the atoms. This makes computations easier and more accurate as divisors (distances) are larger. Pentacene was used as the most basic case for simulations so that the precision and accuracy of these simulations could be used as an upper bound. Additionally, the time scale for Gaussian calculations on pentacene are much smaller than later molecules allowing for more variations to be tried and errors to be less costly.

2.2 Anthradithiophene (ADT-TES-F)

ADT-TES-F, Figure 2.2, is the current benchmark for organic semiconductors. ADT-TES-F is a small, solution processable molecule. Experiments have shown the highest occupied molecular orbital to be -5.35 eV, the lowest unoccupied molecular orbital to be -3.05 eV, the absorption gap to be 528 nm and polycrystalline films characterized by organic field effect transistor hole mobilities between 0.05 and 5.4 $cm^2/(V\cdot s)$ depending on film fabrication methods [23]. This molecule is included because of a considerable amount of experimental data available.

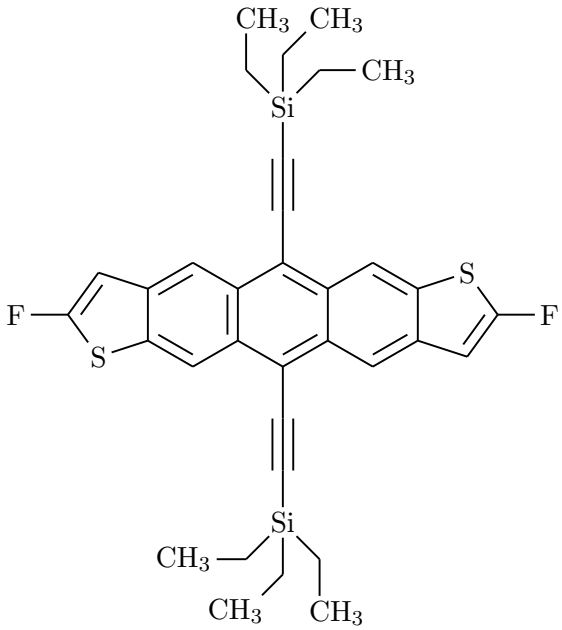

Figure 2.2: Structure of the ADT-TES-F molecule

2.3 peri-Xanthenoxanthene (PXX)

PXX, Figure 2.3, is the core of xylindein. It has already shown promising results for hole mobilities already with 3,9-diphenyl-PXX and 3,9-bis(p-propylphenyl)-PXX showing hole mobilities of up to 0.9 $cm^2/(V \cdot s)$. Additionally, thin film transistor performance for PXX has a significantly higher stability when in contact with oxygen than that which was observed for Pentacene [24, 25]. PXX was chosen due to the presence of experimental data, the structural similarity to xylindein, and its similar shape to that of xylindein.

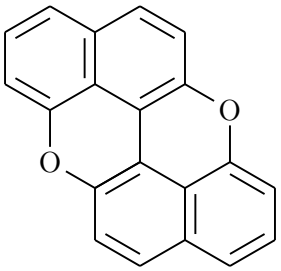

Figure 2.3: Structure of the PXX molecule

PXX is not a computationally simple molecule. Compared to pentacene, it spans two dimensions and contains oxygen in addition to the carbon and hydrogen that were already present. Oxygen, being noticeably more electronegative than carbon and hydrogen, reconfigures the electron cloud towards it creating smaller divisors and thus increasing error and/or computation time. Oxygen also breaks conjugation length, the effective space where the electron is allowed.

2.4 Xylindein

Xylindein, Figure 2.4, is a blue-green pigment that is secreted by the wood-staining fungi *Chlorociboria aeruginosa* and *Chlorociboria aeruginascens*. Xylindein is a low toxicity candidate to be an organic semiconductor that is naturally occurring and therefore does not have to and cannot be synthesized. Successful implementation of xylindein as an organic semiconductor would move towards superior and sustainable semiconductor based devices. Xylindein is relatively unstudied and therefore its properties are unknown.

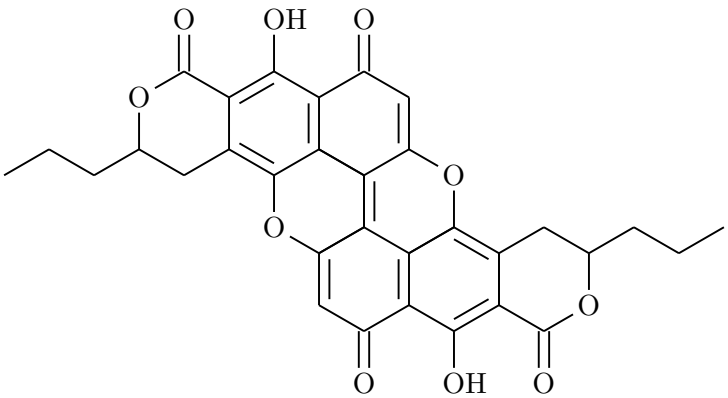

Figure 2.4: Structure of the Xylindein molecule

3 Experimental Methods

To show that xylindein could be useful in organic solar cells and other devices, its characteristics must be determined. Experiments will be used to determine its current-voltage characteristics and photoresponse. The current-voltage characteristics will be used to determine charge carrier mobility. The absorption and fluorescence are used to determine energy levels and to check for Kasha's rule violation.

3.1 Deposition

This section describes the different deposition techniques used.

3.1.1 Drop Casting

Drop casting is a method used to create thin films of solutions. One simply uses a pipette to drop a molecule that is in solution onto a substrate. One does this to create a wide, thick film as the solvent evaporates. Drop casting can make much better films than spin casting because the thickness at the center can be far thicker than the thickness on the edge created by spin casting. The downside of drop casting is that the films one creates are very much distinct from each other in that making the same film twice is difficult/impossible.

3.1.2 Spin Casting

Spin casting is where one drop casts quickly onto a spinning substrate and then lets the substrate continue to spin after the deposition is complete. This creates more consistent films as there will be a thick ring of the sample further out and a thinner sample in the center. This does not create a large concentration of the sample and therefore can produce weaker results when testing with lasers or electrodes where having a thick film the size of the laser is important.

3.2 Characterization

Film and solutions were characterized by experiments for optical absorption spectra, fluorescence spectra, and current vs voltage sweeps. This section will discuss the experiments for all of these.

3.2.1 Optical Absorption

Measurements for optical absorption spectra of thin films and solutions used the light from a tungsten source. This light was sent through a fiber optic cable at normal incidence and received by a second fiber optic cable which took the light to a charge-coupled device spectrometer (Ocean Optics). Thin films and solutions were made both with xylindein and without xylindein so that their spectra could be compared.

3.2.2 Fluorescence

Measurements for fluorescence spectra were taken for thin films and solutions. A laser is incident on the sample and a parabolic mirror is used to collect the light and direct through a filter and then into a spectrometer. The filter is typically a long pass filter which transmits all wavelengths of light higher than a given wavelength and blocks the rest. This is used so that the laser light itself does not show up in the spectrum.

3.2.3 Current-Voltage

Current-voltage characteristics are found by using a thin film from a molecule to bridge the spatial gap across an electrode pair, applying a voltage difference across the electrode pair, and measuring the current going through the circuit. An interdigitated electrode is made out of some conductive material, gold or aluminium for example. The design is such that long thin lines of the material are a small distance apart, on the scale of micrometers. The thin film is then used to connect the two sides of the electrode as a circuit. The material used for the electrode are chosen based on the molecule which is to be used. For xylindein, gold interdigitated electrodes with 10 pairs and 25 μm spacing were used. A Keithley 237 Source-Measure Unit was used as the voltage source. Photoresponse was measured at 400 nm, 532 nm, and 633 nm.

4 Computational Methods

Not all the characteristics of xylindein could be experimentally determined. Computation makes up for this shortcoming. Computational methods will be used to determine the gap energy so that the correct choice of electrode may be used for the current-voltage experiment. Finally, computational methods will be used to determine energy levels to compare with that of the experimental values.

4.1 Gaussian

The computational methods used in this research relied on the Gaussian 09 software suite. Gaussian 09 is a computational chemistry software suite that allows for modeling solid state properties and molecular structure. Gaussian uses fundamental laws of quantum mechanics for its predictions and one can choose to incorporate semi-empirical methods. Guassian 09 is used in tandem with a molecule drawing software such as GaussView 5 or Avogadro. This project used Avogadro as it was found to have more functions.

4.2 Basis Sets

Basis sets are used in computational chemistry to approximate molecular orbitals. Basis sets can be chosen to be any set of orthogonal functions. However, they are not useful unless they are optimized so that error is reduced as much as possible while still allowing for calculations to be done on a reasonable time scale. In this case, a reasonable time frame is less than three days. Slater type functions,

$$S\left(\vec{r}\right) = \alpha_1 e^{-\alpha_2(|\vec{r}|-\alpha_3)} \tag{4.1}$$

where α_1, α_2 and α_3 are used to fit initial conditions, fit molecular orbitals the best but are very computationally extensive as, when in rectangular coordinates, there is a square root in the exponent. Sums of Gaussian functions are more commonly chosen to approximate orbitals. Gaussian functions are of the form

$$G\left(\vec{r}\right) = \beta_1 e^{-\beta_2(\vec{r}\cdot\vec{r}-\beta_3)} \tag{4.2}$$

where β_1, β_2 and β_3 are used to fit initial conditions where there is no longer a squareroot in the exponent when in cartesian coordinates. A sum of Gaussian functions can be more rapidly calculated than the single exponential in the Slater type orbital so they are used to approximate that exponential. The main difference, graphically, between these two functions is the near $|\vec{r}| = 0$ behavior [26]. Figure 4.1 demonstrates the differences between a Gaussian type function and a Slater type function. It also shows how three Gaussian functions can very neatly fit one Slater function.

The fastest basis set simply approximates the Slater exponential with "n" Gaussian functions and they are represented by STO-nG. This is called a minimal basis set. STO-6G predicts the gap energy for PXX, Figure 2.3, to be 9.72 eV but the experimental gap is 2.7 eV [28]. While this method may work for calculating something simple such as the energy levels of hydrogen, STO-6G is not good enough for molecules that are complicated such as xylindein.

Polarization and diffuse functions are common additions to the minimal basis sets. Polarization functions allow for more nodes than the minimalist set. With just Slater functions, one can only create the s-type orbitals of Hydrogen due to the number of nodes. To get higher orbitals, one must add more nodes to the wave function. The notation (d) symbolizes the addition of

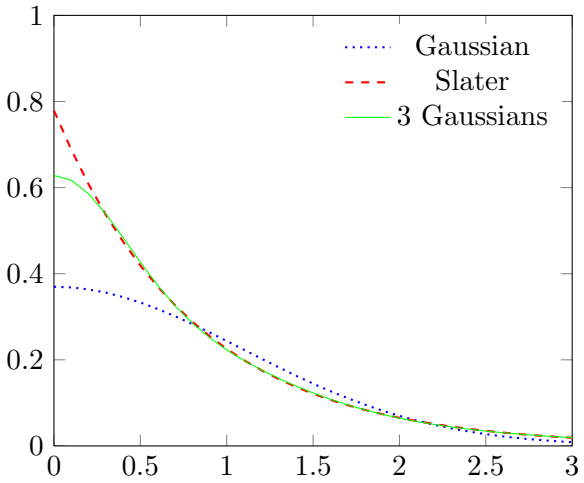

Figure 4.1: Comparison of Gaussian functions and Slater functions [27]

d-type and f-type functions where necessary (d for everything except hydrogen and f-type for transition metals). The notation (p) symbolizes the addition of p-type orbitals to hydrogen. Diffuse functions allow for the electron to create diffuse orbitals where the electron is allowed to be less localized. The notation '++' applies diffuse functions to all atoms and '+' to atoms other than hydrogen.

Split-valence basis sets incorporate the fact that valence electrons are the main factor in bonding whereas minimal sets ignore this. The valence orbitals are now represented by Slater function which are approximated by Gaussian functions. An example of the notation used is 6-311G where the 6 represents the number of Gaussian functions representing the core orbital Slater function, the sequence of numbers after the dash denotes how many Slater functions will be used to approximate the the valence orbital where the n-th number indicates the n-th Slater function. 6-311++G(d,p) predicts PXX, Figure 2.3, to have a gap energy of 3.1 eV. This is reasonable accuracy which could be used in calculations.

4.3 Geometry Optimization

Molecules drawn in Avogadro are not in their lowest energy state. The drawing programs mentioned both have built in Hartree-Fock optimizations that can be run very quickly so that the molecule is much closer to the lowest energy state. This is necessary for quasi-Newtonian methods but, for any complicated molecule, is not close enough to the lowest energy state to be usable in calculations. Hartree-Fock was shown in the previous section to be fast but inaccurate. Gausssian 09 uses a given basis sets to search for a local minimum for the energy with options that will allow the user to go to greater lengths to avoid saddle points.

The geometry optimization uses the Berny algorithm. This algorithm is a quasi-Newtonian algorithm as it assumes a nearly quadratic potential energy surface. Therefore, if the current state of the molecule is "far" from optimization, this method will not work. However, if one is close to the correct geometry, then the series expansion of the potential energy surface will have a first order term of nearly zero as it is close to a minimum or saddle. This makes the series expansion,

$$E(\vec{r}) = a_0 + a_1(\vec{r} - \vec{r}_0) + a_2(\vec{r} - \vec{r}_0)^2 + a_3(\vec{r} - \vec{r}_0)^3 + ..., \tag{4.3}$$

have $a_1 \approx 0$ and, because $\vec{r}$ is close to $\vec{r}_0$, $(\vec{r}-\vec{r}_0)^2 >> (\vec{r}-\vec{r}_0)^3$ as $\vec{r}-\vec{r}_0 << 1$ and therefore the quadratic approximation is valid. The Berny algorithm then uses the Hessian matrix, the matrix of second derivatives of the energy, to find the position where the energy is at a minimum. Again, using a different method to calculate the initial Hessian, such as a Hartree-Fock, speeds up this process greatly [29].

4.4 Methods

Pseudo random calculations led to the choice of B3LYP as a basis set due to its apparent accuracy and speed. To determine the reliability of this basis set, theoretical predictions for pentacene, Figure 2.1, were the first to be computed as experimental values were readily available and the molecule itself is simple. Computations for the last[first] five occupied[unoccupied] energy levels and the excitation wavelengths will be computed and compared. After finishing the comparison for pentacene, a comparison for PXX, Figure 2.3, will be done as PXX will test Gaussian on a molecule with oxygen, PXX is the core of xylindein, and PXX has known experimental values. Finally, the same computations on xylindein itself will be carried out.

5 Results

This section presents fluorescence spectra, absorption spectra, and photocurrent for xylindein and current-voltage characteristics for xylindein and ADT-TES-F. Predicted HUMO levels, LUMO levels, gap energies, and excited states for pentacene, PXX, and xylindein are then presented.

5.1 Experimental Results

Fluorescence was taken for films of xylindein at different wavelengths of excitation. The fluorescence emitted was sent through a long pass filter before getting collected. Data for xylindein in chlorobenzene of unknown concentration is presented in Figure 5.1. Here, the 355 nm used a 480 LP filter and the 633 nm used a 640 nm LP filter. The main peak is shifted roughly 60 nm between them. Furthermore, there are two peaks near the main peak for the 355 nm excitation while there are only two peaks for the 633 nm excitation.

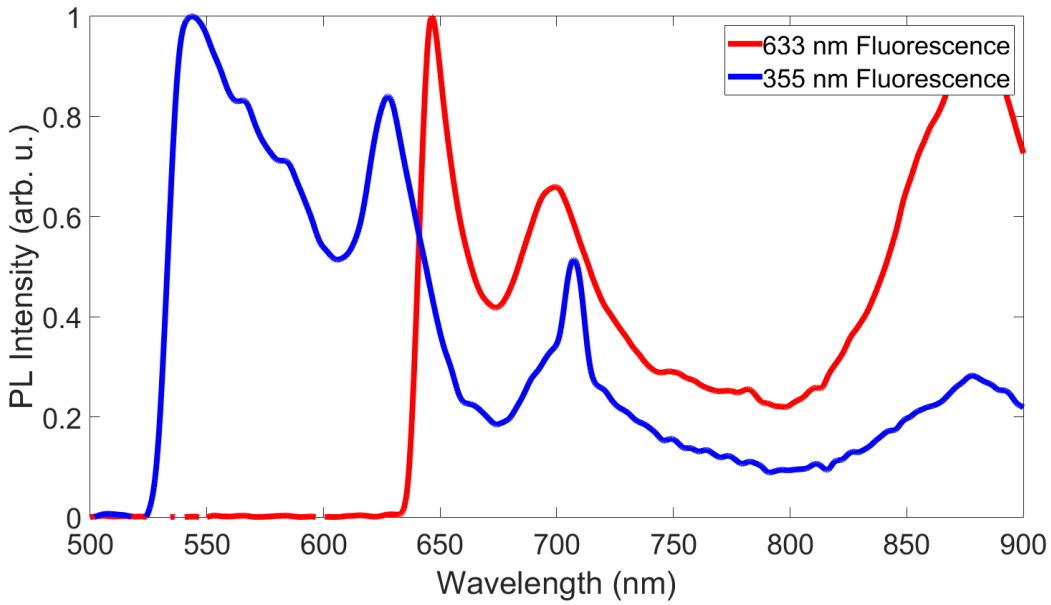

Figure 5.1: Plot of xylindein's fluorescence as a function of wavelengths

Absorption was measured for xylindein in solution and in films. Absorption for films was measured for various deposition temperatures where the film was cast and immediately removed from heat. Additionally, the films were made in contact with oxygen. Figure 5.2 shows absorption as a function of the deposition temperature for thin films made on glass slides. The locations of the peaks do not change between the samples except for the film made at $250° \pm 10°$. This shows that xylindein is stable at temperatures of at least 200°C and that xylindein is stable in contact with oxygen.

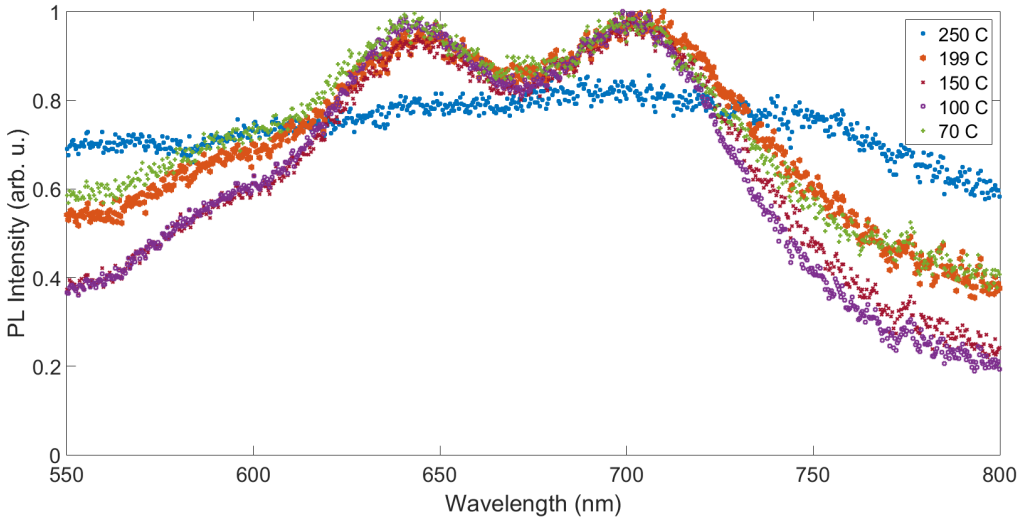

Figure 5.2: Plot of xylindein's absorption as a function of temperature

Figure 5.3 shows absorption as a function of annealing time for several temperatures for thin films made on glass slides. The annealing time is how long the sample remained in contact with the heat plate until it was removed. Again, the films were made in contact with oxygen. The lack of change in peak location supports the ability for xylindein to not degrade in the presence of oxygen or heat further.

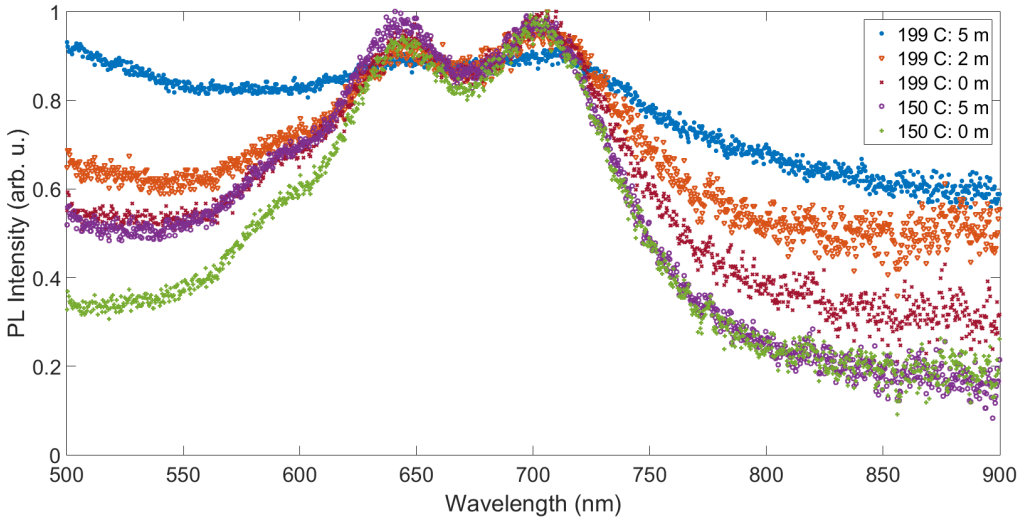

Figure 5.3: Plot of xylindein's absorption as a function of annealing time

Figure 5.4 compares absorption to fluorescence. Both spectra were taken from the same sample which was in solution. The expectation from a typical molecule would be that the absorption would be a mirror image about a vertical line shifted to the left of the main peak of the fluorescence. This is not the case. The absorption has a higher wavelength, and not a smaller one, than that of the main peak. The fluorescence also has more peaks than did the absorption.

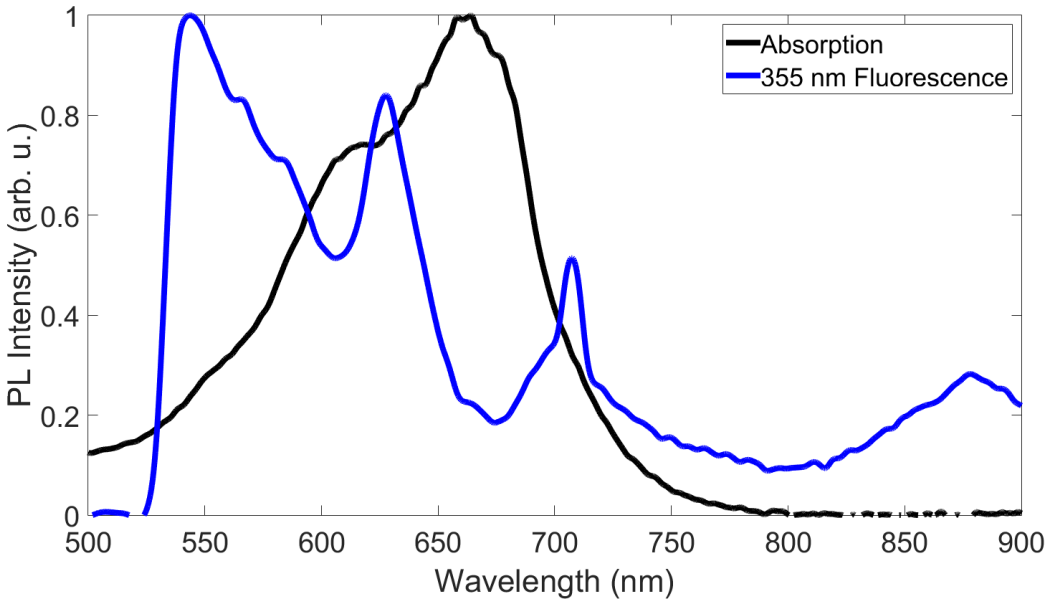

Figure 5.4: Plot of xylindein's absorption and fluorescence

A current-voltage data sweep was measured for xylindein on gold, interdigitated electrodes. This data is presented in Figure 5.5. Figure 5.5 also shows photoresponse at three different wavelengths. A lower estimate for the charge carrier mobility was determined from the quadratic regimes of the current.

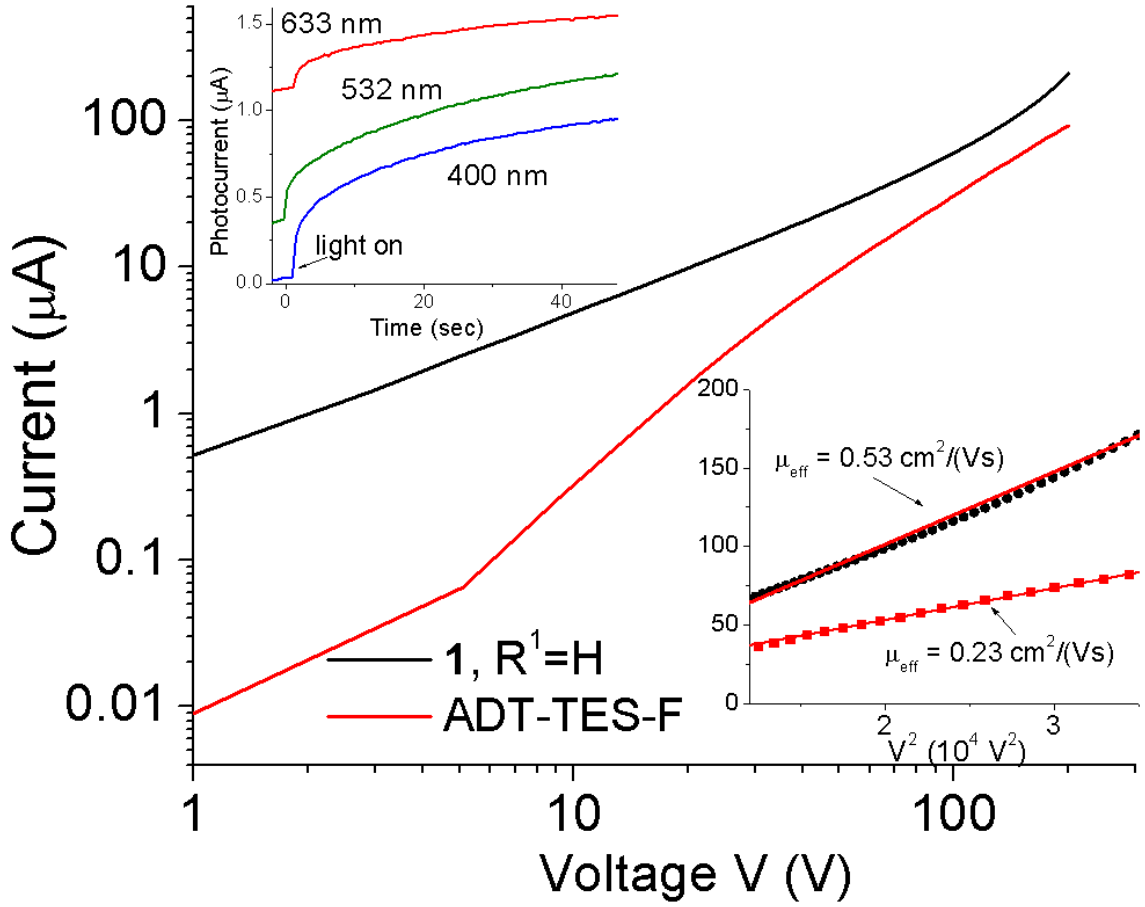

Figure 5.5: Plot of xylindein and ADT-TES-F's current-voltage characteristics

5.2 Computational Results

This section presents the computational and experimental values for the HOMO levels, LUMO levels, gap energies, and excited states for pentacene, pxx, and xylindein. These results are then summarized at the end.

5.2.1 Pentacene

Gaussian predicted the highest occupied molecular orbital to be at -4.4 eV and the lowest unoccupied molecular orbital at -2.6 eV. Experimental values were lower for both, -4.9 eV for HOMO and -2.9 eV for LUMO [23]. The gap energy prediction for pentacene was 1.8 eV while the experimental was 2.0 eV. The first two excited state wavelengths were then computed (Computation: 783 nm, 473 nm — Experimental: 590 nm, 360 nm [23]). Both excited states were overestimated.

5.2.2 PXX

Gaussian predicted the HOMO to be at -4.9 eV and the LUMO at -1.8 eV. Experimental values were larger for both, -5.0 eV for HOMO and -2.3 eV for LUMO [28]. The gap energy prediction for PXX was 3.1 eV while the experimental was 2.7 eV. The first excited state wavelength was then computed (Computation: 462 nm — Experimental: 445 nm [28]). This excited state was also overestimated.

5.2.3 Xylindein

Gaussian predicted the HOMO to be at -6.5 eV and the LUMO at -4.1 eV. The gap energy prediction for xylindein was 2.4 eV. This first excited state was then calculated (Computation: 584 nm — Experimental: 680 nm). This time, however, the excited state was underestimated.

5.2.4 Summary

The computational and experimental, where applicable, data is presented in Figure 5.6. One can notice that for pentacene and PXX, the excited states were overestimated. This trend was also obvserved with other tested and not reported molecules. This trend is consistent with theoretical work [30]. Xylindein, however, is underestimated.

	HOMO c(e)	LUMO c(e)	1st Excited c(e)
Pentacene	-4.4 eV(-4.9 eV)	-2.6 eV(-2.9 eV)	783 nm(590 nm)
PXX	-4.9 eV(-5.0 eV)	-1.8 eV(-2.3 eV)	462 nm(445 nm)
Xylindein	-6.5 eV	-4.1 eV	584 nm(680 nm)

Figure 5.6: Comparison of computational and experimental data

6 Discussion

This section will discuss the experimental and computational data that was taken and presented.

6.1 Computational Results

The computational results for pentacene and PXX show how reliable Gaussian's predictions can be taken. Data for these two molecules shows a trend for a small overestimation of both the HOMO and LUMO energy levels. However, this overestimation is rather consistent causing the gap energy to be within 15% of the experimental value. However, the predicted values for excitation wavelength are much less usable for anything but an upper bound as the error in the tested cases are far too large. Again, Gaussian tended to overestimate the wavelengths which agrees with theory [30] for all molecules tested except xylindein.

In Appendix A, a rough estimation for where xylindein's first excitation wavelength should be is performed. This produces a value of 723.15 nm. For pentacene, the experimental value was significantly red-shifted from the estimated value. The computational value for the peak is significantly red-shifted from the estimated value but the experimental value is not. This leads to the possibility that the experimental values are not actually for xylindein but, instead, for clumps of xylindein molecules brought about by the strong inter-molecular bonds that xylindein creates. This phenomenon is common in pigments.

6.2 Kasha's Rule

Figure 5.1 shows how the fluorescence peaks change when the excitation wavelength changes. This would seem to contradict Kasha's rule as it implies that the fluorescence will always occur from the $S_1 \rightarrow S_0$ transition. Furthermore, Figure 5.4 shows that the absorption is not a mirror image of the fluorescence which is also an indication of a violation of Kasha's rule.

The data at hand is ambiguous as to whether Kasha's rule is indeed violated or held. While the data clearly shows wavelength dependence on fluorescence and the absorption is not a mirror of the fluorescence as it should be, the present data has been determined to not actually be for isolated xylindein molecules. Experiments wherein small clumps of xylindein molecules, as is a common occurrence in pigments, are present would have a similar outcome of wavelength dependent fluorescence. Hydrogen bonding and pi-stacking would both play a role in increasing the probability of these clumps forming.

6.3 Mobility

Figure 5.5 shows the current as a function of voltage for ADT-TES-F and xylindein. Both of these functions start in a linear regime and transition to a quadratic regime, ADT-TES-F transitions at ~ 5 V and xylindein transitions at ~ 120. The scaling factor of the quadratic regime is proportional to the charge carrier mobility. A lower bound for the charge carrier mobility was estimated to be 0.53 $\frac{\text{cm}^2}{\text{V s}}$ for xylindein and 0.23 $\frac{\text{cm}^2}{\text{V s}}$ for ADT-TES-F.

7 Conclusion

The full capabilities of xylindein are still not fully understood, but xylindein does have a few important characteristics for organic semiconductors. Xylindein is stable in oxygen and at high temperatures as Figures 5.2-5.4 indicate. Furthermore, experiments show a lower estimate for charge carrier mobility to be 0.5 $\frac{\text{cm}^2}{\text{V s}}$ in amorphous films which is on par with similarly processed crystalline films.

Future research in this project will include taking reproducible data sets for current-voltage characteristics on co-planar electrodes. Data needs to be taken for xylindein in ordered films such as those that would be spin cast. Finally, xylindein will be used as a donor in donor-acceptor combinations to make solar cells and in single-component solar cells. The power conversion efficiencies will then be measured and compared to current benchmarks.

8 Acknowledgements

First and foremost is my thesis advisor, Professor Oksana Ostroverkhova, who guided and assisted me whenever and wherever I needed. I would like to also acknowledge Dr. Brian Johnson who trained me and aided me with experimental procedures and my fellow physics 403 classmates who peer reviewed this work. Funding from URISC allowed the research to be continued over the summer of 2015.

9 Appendix: Conjugation Length

One can roughly estimate the excited states' wavelength for a molecule by approximating it as an electron in a box where the length is the conjugation length. The conjugation length is the effective space where electron is allowed. Then one can simply compute change in the energy by

$$\Delta E_{n,n+k} = \frac{h^2}{8mL^2}\left[(n+k)^2 - n^2\right] = \frac{h^2}{8mL^2}\left(2nk + k^2\right) \tag{9.1}$$

and, because electrons occupy states as pairs, the N levels that are going to be filled only go up to $n = {}^{N}/_{2}$ where N is the number of molecules in the chain. Therefore, Equation 9.1 becomes

$$\Delta E = \frac{h^2}{8mL^2}\left(Nk + k^2\right). \tag{9.2}$$

Molecules were drawn in Avogadro and optimized to be in their lowest energy state. The parameter, L, was then determined by measuring the longest chain of atoms in the molecule. For pentacene, the distance is 1.7597 nm. For xylindein, the distance is 1.8137 nm. The parameter, m, is the mass of an electron. The transition from the first excited state to the ground state is the transition in question which means that $k = 1$. N is the number of molecules making up the box and it is 15 for pentacene and 14 for xylindein. Using this method, one predicts the first excited state for pentacene to be at 680.73 nm which is significantly red-shifted from the experimental value of 590 nm. This method also gives 723.15 nm for xylindein.

10 Bibliography

[1] S. D. Dimitrov and J. R. Durrant, "Materials Design Considerations for Charge Generation in Organic Solar Cells," *Chemistry of Materials*, vol. 26, pp. 616–630, Jan. 2014. 4

[2] L. Dou, J. You, Z. Hong, Z. Xu, G. Li, R. A. Street, and Y. Yang, "25th Anniversary Article: A Decade of Organic/Polymeric Photovoltaic Research," *Advanced Materials*, vol. 25, pp. 6642–6671, Dec. 2013. 4

[3] B. Minaev, G. Baryshnikov, and H. Agren, "Principles of phosphorescent organic light emitting devices," *Physical Chemistry Chemical Physics*, vol. 16, pp. 1719–1758, Jan. 2014. 4

[4] I. D. W. Samuel and G. A. Turnbull, "Organic Semiconductor Lasers," *Chemical Reviews*, vol. 107, pp. 1272–1295, Apr. 2007. 4

[5] S. Köber, M. Salvador, and K. Meerholz, "Organic Photorefractive Materials and Applications," *Advanced Materials*, vol. 23, pp. 4725–4763, Nov. 2011. 4

[6] B. Lynn, P.-A. Blanche, and N. Peyghambarian, "Photorefractive polymers for holography," *Journal of Polymer Science Part B: Polymer Physics*, vol. 52, pp. 193–231, Feb. 2014. 4

[7] P.-A. Blanche, A. Bablumian, R. Voorakaranam, C. Christenson, W. Lin, T. Gu, D. Flores, P. Wang, W.-Y. Hsieh, M. Kathaperumal, B. Rachwal, O. Siddiqui, J. Thomas, R. A. Norwood, M. Yamamoto, and N. Peyghambarian, "Holographic three-dimensional telepresence using large-area photorefractive polymer," *Nature*, vol. 468, pp. 80–83, Nov. 2010. 4

[8] S. Tay, P.-A. Blanche, R. Voorakaranam, A. V. Tunç, W. Lin, S. Rokutanda, T. Gu, D. Flores, P. Wang, G. Li, P. St Hilaire, J. Thomas, R. A. Norwood, M. Yamamoto, and N. Peyghambarian, "An updatable holographic three-dimensional display," *Nature*, vol. 451, pp. 694–698, Feb. 2008. 4

[9] I. Etxebarria, J. Ajuria, and R. Pacios, "Polymer:fullerene solar cells: materials, processing issues, and cell layouts to reach power conversion efficiency over 10%, a review," *Journal of Photonics for Energy*, vol. 5, no. 1, pp. 057214–057214, 2015. 4

[10] Y. Cao, Y. Liang, L. Zhang, S. Osuna, A.-L. M. Hoyt, A. L. Briseno, and K. N. Houk, "Why Bistetracenes Are Much Less Reactive Than Pentacenes in Diels–Alder Reactions with Fullerenes," *Journal of the American Chemical Society*, vol. 136, pp. 10743–10751, July 2014. 4

[11] G. Priebe, B. Pietzak, and R. Könenkamp, "Determination of transport parameters in fullerene films," *Applied Physics Letters*, vol. 71, pp. 2160–2162, Oct. 1997. 4

[12] R. Dattani, K. F. Gibson, S. Few, A. J. Borg, P. A. DiMaggio, J. Nelson, S. G. Kazarian, and J. T. Cabral, "Fullerene oxidation and clustering in solution induced by light," *Journal of Colloid and Interface Science*, vol. 446, pp. 24–30, May 2015. 4

[13] O. K. Kwon, J.-H. Park, D. W. Kim, S. K. Park, and S. Y. Park, "An All-Small-Molecule Organic Solar Cell with High Efficiency Nonfullerene Acceptor," *Advanced Materials*, vol. 27, pp. 1951–1956, Mar. 2015. 4

[14] X. Zhang, C. Zhan, and J. Yao, "Non-Fullerene Organic Solar Cells with 6.1% Efficiency through Fine-Tuning Parameters of the Film-Forming Process," *Chemistry of Materials*, vol. 27, pp. 166–173, Jan. 2015. 4

[15] J. Zhao, Y. Li, H. Lin, Y. Liu, K. Jiang, C. Mu, T. Ma, J. Y. L. Lai, H. Hu, D. Yu, and H. Yan, "High-efficiency non-fullerene organic solar cells enabled by a difluorobenzothiadiazole-based donor polymer combined with a properly matched small molecule acceptor," *Energy & Environmental Science*, vol. 8, pp. 520–525, Feb. 2015. 4

[16] S. Sutty, G. Williams, and H. Aziz, "Fullerene-based Schottky-junction organic solar cells: a brief review," *Journal of Photonics for Energy*, vol. 4, p. 040999, May 2014. 4

[17] N. Camaioni and R. Po, "Pushing the Envelope of the Intrinsic Limitation of Organic Solar Cells," *The Journal of Physical Chemistry Letters*, vol. 4, pp. 1821–1828, June 2013. 4

[18] S. Torabi, F. Jahani, I. Van Severen, C. Kanimozhi, S. Patil, R. W. A. Havenith, R. C. Chiechi, L. Lutsen, D. J. M. Vanderzande, T. J. Cleij, J. C. Hummelen, and L. J. A. Koster, "Strategy for Enhancing the Dielectric Constant of Organic Semiconductors Without Sacrificing Charge Carrier Mobility and Solubility," *Advanced Functional Materials*, vol. 25, pp. 150–157, Jan. 2015. 4

[19] E. D. Głowacki, L. Leonat, M. Irimia-Vladu, R. Schwödiauer, M. Ullah, H. Sitter, S. Bauer, and N. S. Sariciftci, "Intermolecular hydrogen-bonded organic semiconductors—Quinacridone versus pentacene," *Applied Physics Letters*, vol. 101, p. 023305, July 2012. 4

[20] M. Nič, J. Jirát, B. Košata, A. Jenkins, and A. McNaught, eds., *IUPAC Compendium of Chemical Terminology: Gold Book*. Research Triagle Park, NC: IUPAC, 2.1.0 ed., June 2009. 5

[21] P. Klán and J. Wirz, *Photochemistry of Organic Compounds: From Concepts to Practice*. John Wiley & Sons, Mar. 2009. 5

[22] D. González-Rodríguez and A. P. H. J. Schenning, "Hydrogen-bonded Supramolecular π-Functional Materials," *Chemistry of Materials*, vol. 23, pp. 310–325, Feb. 2011. 5

[23] A. D. Platt, J. Day, S. Subramanian, J. E. Anthony, and O. Ostroverkhova, "Optical, Fluorescent, and (Photo)conductive Properties of High-Performance Functionalized Pentacene and Anthradithiophene Derivatives," *The Journal of Physical Chemistry C*, vol. 113, pp. 14006–14014, Aug. 2009. 6, 7, 19

[24] N. Kobayashi, M. Sasaki, and K. Nomoto, "Stable peri-Xanthenoxanthene Thin-Film Transistors with Efficient Carrier Injection," *Chemistry of Materials*, vol. 21, pp. 552–556, Feb. 2009. 8

[25] L. Wang, G. Duan, Y. Ji, and H. Zhang, "Electronic and Charge Transport Properties of peri-Xanthenoxanthene: The Effects of Heteroatoms and Phenyl Substitutions," *The Journal of Physical Chemistry C*, vol. 116, pp. 22679–22686, Nov. 2012. 8

[26] A. Tomberg, "Gaussian 09w tutorial," 2015. 11

[27] E. G. Lewars, *Computational Chemistry: Introduction to the Theory and Applications of Molecular and Quantum Mechanics*. Springer Science & Business Media, Nov. 2010. 12

[28] N. Lv, M. Xie, W. Gu, H. Ruan, S. Qiu, C. Zhou, and Z. Cui, "Synthesis, properties, and structures of functionalized peri-xanthenoxanthene," *Organic Letters*, vol. 15, pp. 2382–2385, May 2013. 11, 19

[29] D. Young, *Computational Chemistry: A Practical Guide for Applying Techniques to Real World Problems*. John Wiley & Sons, Apr. 2004. 13

[30] K. Kahn and B. Kirtman, "Configuration Interaction Singles for Excited States." `http://people.chem.ucsb.edu/kahn/kalju/chem126/public/elspect_cis.html`. 19, 20